**Steel and Composite Structures**, *Vol. 32, No. 4 (2019) 443-454*
DOI: https://doi.org/10.12989/scs.2019.32.4.443


# Theoretical and experimental study on shear strength of precast steel reinforced concrete beam

Yong Yang [1], Yicong Xue *[1,2] and Yunlong Yu [1,3]

[1] *School of Civil Engineering, Xi'an University of Architecture and Technology, Shaanxi, China*
[2] *School of Natural and Built Environment, Queen's University Belfast, Northern Ireland, UK*
[3] *Key Lab of Structure and Earthquake Resistance, Shaanxi, China*

(*Received May 5, 2018, Revised March 11, 2019, Accepted July 30, 2019*)

**Abstract.** With the aim to put forward the analytical model for calculating the shear capacity of precast steel reinforced concrete (PSRC) beams, a static test on two full-scale PSRC specimens was conducted under four-point loading, and the failure modes and strain developments of the specimens were critically investigated. Based on the test results, a modified truss-arch model was proposed to analyze the shear mechanisms of PSRC and cast-in-place SRC beams. In the proposed model, the overall shear capacity of PSRC and cast-in-place SRC beams can be obtained by combining the shear capacity of encased steel shape with web concrete determined by modified Nakamura and Narita model and the shear capacity of reinforced concrete part determined by compatible truss-arch model which can consider both the contributions of concrete and stirrups to shear capacity in the truss action as well as the contribution of arch action through compatibility of deformation. Finally, the proposed model is compared with other models from JGJ 138 and AISC 360 using the available SRC beam test data consisting of 75 shear-critical PSRC and SRC beams. The results indicate that the proposed model can improve the accuracy of shear capacity predictions for shear-critical PSRC and cast-in-place SRC beams, and relatively conservative results can be obtained by the models from JGJ 138 and AISC 360.

**Keywords:** steel reinforced concrete beams; precast concrete; shear capacity; modified truss-arch model; experimental study

## 1. Introduction

As an important part of steel-concrete composite structures, steel reinforced concrete structures (SRCs) have been widely applied in high-rise structures and large-span structures (Huang *et al.* 2019, Liang *et al.* 2019, Chu *et al.* 2018, Chen and Liu 2018, Nzabonimpa *et al.* 2018, Rana *et al.* 2018, Yan *et al.* 2017, Xiao *et al.* 2017, Massone *et al.* 2017, Elmy and Nakamura 2017, Zhu *et al.* 2017, Ma *et al.* 2016). However, the application of cast-in-place SRC structures has been limited in conventional residential and public buildings because of the complexity in construction period. The construction of SRC structures involves both the construction procedure of steel structures and concrete structures, which will directly increase the construction cost. Therefore, some researchers (Yang *et al.* 2016, 2017, 2018, Nzabonimpa *et al.* 2017, Kim *et al.* 2013) have suggested the combination of SRC structures and precast structures to facilitate the construction process and to improve the mechanical performance of conventional cast-in-place SRC structures.

An innovative precast steel reinforced concrete (PSRC) beam is presented in this paper, which is shown in Fig. 1(a). This PSRC beam is composed of a precast outer-part and a cast-in-place inner-part, and the type and strength of concrete in the both parts can be designed differently to meet different purposes. In the precast period, modularized foam formwork is attached on the both sides of the steel web by special glue with a fixed spacing, and concrete diaphragms would form after the high-strength concrete flowed into the gap between the adjacent formwork, as shown in Fig. 2. The high-strength precast outer-part with higher capacity and stiffness could enhance the mechanical performance during the construction period, and the concrete diaphragms could serve as shear connectors to enhance the bonding performance between the precast and cast-in-place concrete. Furthermore, the concrete in the inner-part could be cast with the floor slab at the same time using conventional concrete to enhance the structural integrity and to save the consumption of expensive high-strength concrete. With the aim to propel the application of this PSRC beam, the objective of this paper is to develop an effective method for calculating the load bearing capacities of this PSRC beam.

As well known, shear failure, as a brittle failure mode, should be avoided in the practical applications. Therefore, it becomes the key issue in the design of this PSRC beam to predict the shear capacity accurately. Over the past decades, many design codes (JGJ 138-2016 2016, AISC 360-10 2010) have proposed simplified semi-empirical expressions based on extensive experimental data to predict the shear

*Corresponding author,
Ph.D. Candidate, Visiting Research Associate,
E-mail: xjdxyc@foxmail.com


http://www.techno-press.org/?journal=scs&subpage=6
ISSN: 1229-9367 (Print), 1598-6233 (Online)


(a) Section diagram (b) Design details

Fig. 1 Diagrams of specimens

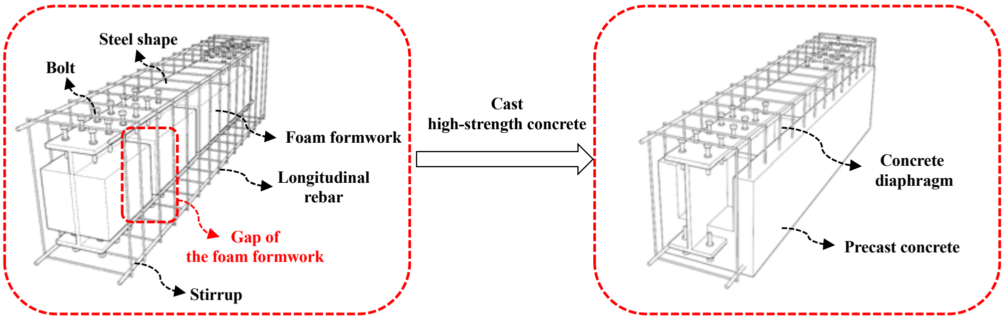


Fig. 2 Diagram of construction process

capacity of SRC beams. However, the models aforementioned are established on the basis of simplified superposition method and regression analysis, in which the shear capacity of a SRC beam can be simply regarded as the sum of the shear capacity of reinforced concrete part based on regression analysis and the shear capacity of steel shape based on von Mises yielding criterion, indicating that these models may lack clear physical meanings, and most of them are relatively or excessively conservative for safety, which may cause the waste of materials and resources.

With the aim to put forward an analytical model for calculating the shear capacity of this PSRC beam, a static test on two full-scale PSRC specimens was conducted under four-point loading. Based on the test results, a proposed model which is based on the shear capacity models of Pan and Li (2013) and Nakamura and Narita (2003) was proposed to analyze the shear mechanism of these PSRC beams. The proposed model can effectively consider the different concrete strengths of the precast outer-part and cast-in-place inner-part and is also suitable for predicting the shear capacity of conventional SRC beams. Finally, the validity of the proposed model was verified using the test data of 75 shear-critical SRC and PSRC beams and it was also compared with other shear models from JGJ 138 and AISC 360 later in this paper.

## 2. Test program

### 2.1 Specimen design

In this study, a static test was conducted on two full-scale specimens to investigate the shear performance of this PSRC beam. The main experimental variable was the shear span aspect ratio. The shear span aspect ratio, defined as the shear span length divided by the effective height of the PSRC beam, which is the distance from the specimen top to the center of tensile longitudinal rebar, varied from 1.0 to 1.5 to investigate the shear behavior with the change of shear span length. The parameters of the specimens are summarized in Table 1.

The section details of the specimens are shown in Fig. 1(b). As illustrated in Fig. 1(b), the height and width of the cross section were 650 mm and 450 mm, respectively. The steel shape in all specimens was HN500×200×9×14 of Q235 grade per the Chinese standard (JGJ 138-2016 2016),

Table 1 Parameters of the specimens

| Specimen ID | $\lambda$ | $a$ (mm) | $h_0$ (mm) | $f_{cu,outer}$ (MPa) | $f_{cu,inner}$ (MPa) | Steel shape ($\rho_{ss}$) | Longitudinal rebar ($\rho_s$) | Stirrup ($\rho_v$) |
|---|---|---|---|---|---|---|---|---|
| PSRC-1 | 1.0 | 600 | 600 | 45.0 | 24.3 | HN500×200×9×14 (3.46%) | 5 25 / 5 25 (1.82%) | 6@80 (0.16%) |
| PSRC-2 | 1.5 | 900 | 600 | 45.0 | 24.3 | | | |

*$\lambda$ is the aspect ratio; $a$ is the shear span; $h_0$ is the effective height; $f_{cu,out}$ is the cubic compressive strength of precast concrete; $f_{cu,in}$ is the cubic compressive strength of cast-in-place concrete

indicating the total height and the width of the steel shape were 500 mm and 200 mm, respectively, and the thickness of its web and flanges were 9 mm and 14 mm, respectively.

### 2.2 Materials

For the flange of the steel shape, the measured tensile strengths were 273 MPa at yield and 432 MPa at peak. For the web of the steel shape, the measured tensile strengths were 317 MPa at yield and 453 MPa at peak. The tested tensile strengths of the longitudinal reinforcement, steel rebar with a diameter of 25 mm and a grade of HRB400, were 443 MPa at yield and 598 MPa at peak. The tested tensile strengths of the stirrup, steel rebar with a diameter of 6 mm and a grade of HPB300, were 393 MPa at yield and 562 MPa at peak.

The cubic compressive strengths of the concrete in the precast outer-part and the cast-in-place inner-part were designed to be different. In all the specimens, the strength grade of the concrete in the outer-part was identical, which was C50 graded according to the Chinese code (GB50010-2010 2010), and the measured cubic compressive strength was 45.0 MPa at 28 days. The strength grade of concrete in the inner-part was designed at C30, and the tested cubic compressive strength at 28 days was 24.3 MPa.

### 2.3 Test instrumentations

As illustrated in Fig. 3, the specimens were tested under four-point loading. A 20000 kN hydraulic jack was used to apply vertically monotonic load through two spreader beams. During the test process, 5 linear variable differential transformers (LVDTs) were employed to monitor deflections of the beam, at mid-point, two loading points, and both ends of the beam. A considerable number of strain gauges were arranged on the web and flanges of the steel shape and the stirrups to monitor the strain response. The layouts of strain gauges and LVDTs are shown in Fig. 4. The test was terminated when the post-peak load-carrying capacity decreased to 85% of the peak load or the vertical displacement at the mid-span was over 70mm for safety.

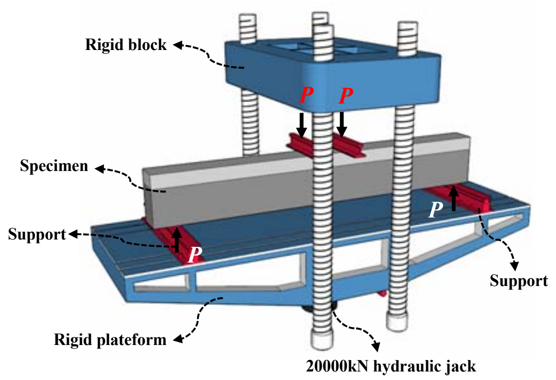


Fig. 3 Test device

## 3. Test results

### 3.1 Failure mode

The failure modes and damage patterns of the specimens are shown in Fig. 5. The typical diagonal compression failure and shear compression failure were found in the specimens PSRC-1 and PSRC-2, respectively. For the specimen PSRC-1, the initial crack could be seen at the mid-span at approximately $0.15P_u$, and inclined cracks initiated at about $0.3P_u$, where $P_u$ is the maximum load which the specimen experienced during the loading process. The formation of a complete diagonal compressive strut could be observed at the end of the test. For the specimen PSRC-2, the crack pattern at the early loading stage was similar to that of the specimen PSRC-1. Inclined cracks initiated at about $0.4P_u$ and propagated as the load increased until the test ended. Vertical cracks at the mid-span propagated slowly and the final failure mode was dominated by the principal diagonal shear crack extending through the critical section. As shown in Fig. 5(b) and Fig. 5(d), no obvious longitudinal cracks which indicated slippage occurred were observed at the final loading stages, indicating that the precast concrete and cast-in-place concrete were well composite.

### 3.2 Load-displacement curves and Load-strain curves

Fig. 6 shows the load-displacement curves at the mid-span point of the specimens. As shown in Fig. 6, the specimen PSRC-1 exhibited a greater initial stiffness than the specimen PSRC-2 due to the lower aspect ratio. The

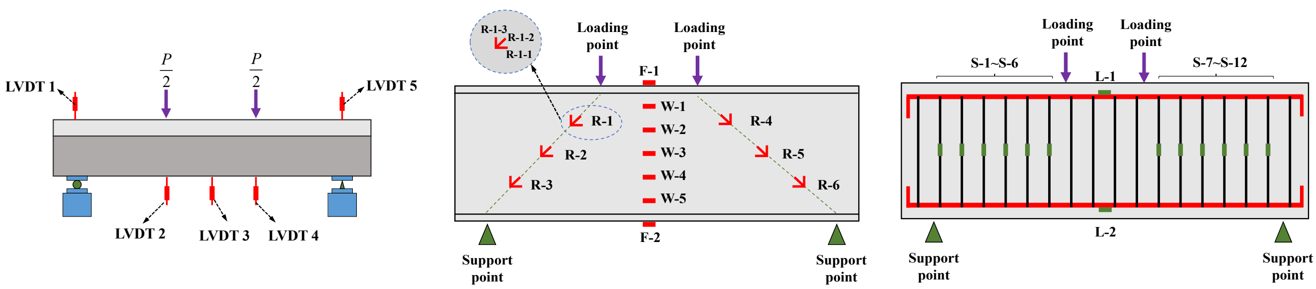


(a) Arrangement of LVDTs

(b) Arrangement of strain gauges on steel shape

(c) Arrangement of strain gauges on steel skeleton

Fig. 4 Layouts of LVDTs and strain gauges

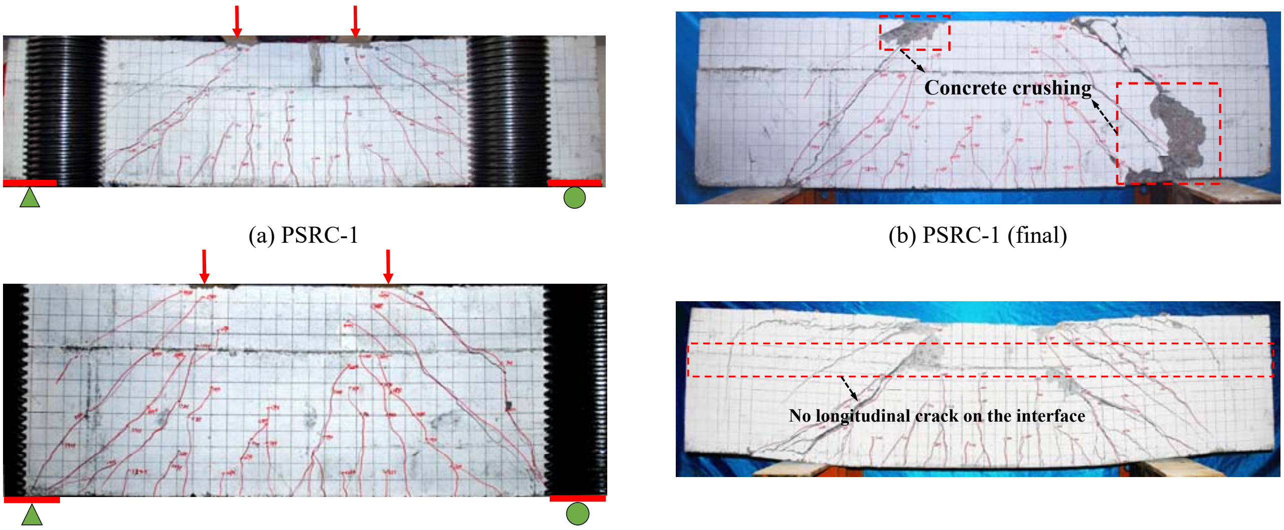


(a) PSRC-1 (b) PSRC-1 (final)

(c) PSRC-2 (d) PSRC-2 (final)

Fig. 5 Failure modes and crack patterns

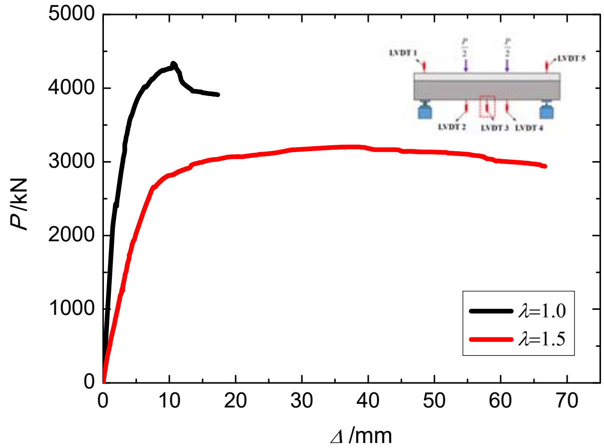


Fig. 6 Load-displacement curves at mid-span

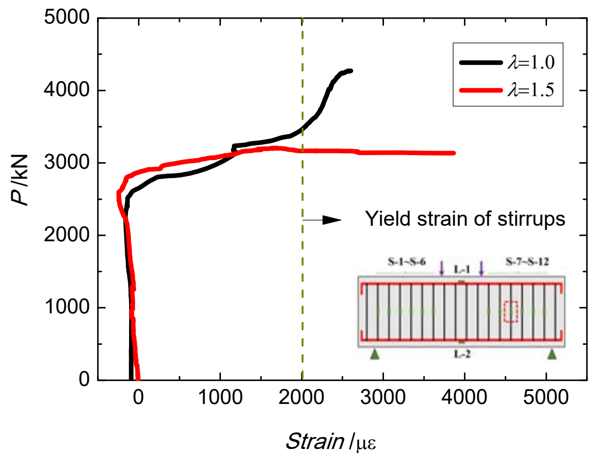


Fig. 7 Load-strain curves of stirrups

specimen PSRC-1 suffered a significant drop of vertical load after the peak load due to the crushing of diagonal concrete strut, and the specimen PSRC-2 which failed in shear compression showed better deformability. From the load-displacement curves, the ductility coefficients of the specimens were determined as listed in Table 2. The ductility coefficient was calculated as the result of the ultimate mid-span displacement $\Delta_u$ divided by the yield mid-span displacement $\Delta_y$. $\Delta_y$ was obtained using the equal energy method (Park 1988) and $\Delta_u$ is the mid-span displacement when the vertical load degraded to $0.85P_u$ or the vertical displacement at the mid-span was over 70 mm.

From the calculated results, it can be seen that the specimen PSRC-2 which failed in shear compression mode exhibited the relatively higher ductility ratio than the specimen PSRC-1 which failed in diagonal compression mode, indicating that the deformability increased with the increasing of aspect ratios. Nevertheless, as shown in Fig. 6, a plateau can be observed after a sudden drop in the load-displacement curve of the specimen PSRC-1 during the post-peak load stage, indicating that the load could be hold steadily if the specimen PSRC-1 could be further tested. The sudden loss in load can be attributed to the concrete crushing after the peak load reached, but the specimen

Table 2 Test results

| ID | $\lambda$ | Failure mode | $P_{cr}$ (kN) | $P_u$ (kN) | $\Delta_{cr}$ (mm) | $\Delta_y$ (mm) | $\Delta_u$ (mm) | $\mu$ |
|---|---|---|---|---|---|---|---|---|
| PSRC-1 | 1.0 | Diagonal compression | 650 | 4340.6 | 0.58 | 6.5 | 17.3 | 2.7 |
| PSRC-2 | 1.5 | Shear compression | 600 | 3200.3 | 0.93 | 10.6 | 66.7 | 6.3 |

*$P_{cr}$ is the crack load; $P_u$ is the peak load; $\Delta_{cr}$ is the crack displacement at the mid-span; $\Delta_y$ is the yield displacement at the mid-span; $\Delta_u$ is the ultimate displacement at the mid-span; $\mu$ is the ductility coefficient

could exhibit a tough post-peak load stage due to the contribution of steel shape and confined web concrete if further loaded.

Fig. 7 shows the load-strain curves of the stirrups, in which the strain history of the gauge S9 was employed here. The results indicated that the stirrups of the specimens yielded before the corresponding peak loads reached, and the tensile strain of the stirrups increased with the development of inclined cracks, indicating that stirrup played an important role in the shear performance of the tested PSRC beams.

## 4. Analytical work of shear capacity

Over the past decades, many researchers have developed sectional models or semi-empirical models on the basis of extensive experimental data to predict the shear capacity of SRC beams. Some researchers proposed modified strut and tie models, which regards the web of steel shape as distributed longitudinal or transverse tie, but in their models, the existence of the steel flanges may disturb or break the formation of concrete compressive strut (Deng *et al*. 2018). Many design codes, such as AISC 360 and JGJ 138, proposed calculation formulas to determine the shear capacity of SRC beams, but most of them are based on the superposition method and regression analysis, which may lack clear physical meanings.

This paper presents an innovative model based on the modified Pan and Li model (2013) and modified Nakamura and Narita model (2003). As illustrated in Fig. 8, the overall shear capacity of a SRC beam can be determined by combining the shear capacity of the steel shape with web concrete and the shear capacity of the reinforced concrete (RC) part. For the steel shape with web concrete, the shear mechanism of this part is similar to that of a partially encased concrete (PEC) member, therefore, the Nakamura and Narita model, which can be used to determine the shear capacity of PEC beams precisely, is employed and modified here. For the RC part, the Pan and Li model, which is based on the compatible truss-arch model, is used here to determine the shear capacity of the RC part. Because the equivalent width of the RC part is defined as the width of the specimen deducting that of the steel flange, the arch action of the RC part may not be broken or disturbed by the steel flanges. Therefore, the shear capacity of a PSRC beam consisting of four parts is expressed as follows

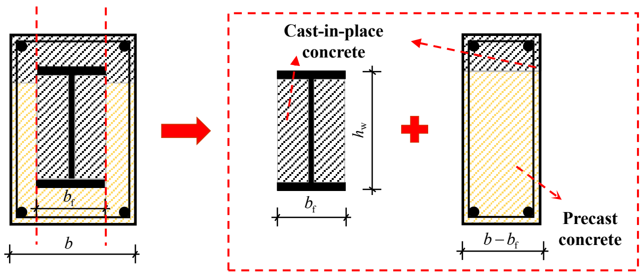


Fig. 8 Calculation diagram

$$V = V_{\rm RC} + V_{\rm ss} = (V_{\rm ct} + V_{\rm s} + V_{\rm a}) + V_{\rm ss} \tag{1}$$

where $V_{\rm ct}$ and $V_{\rm s}$ are the contributions of concrete and stirrups to the shear capacity of truss action, respectively; $V_{\rm a}$ is the shear capacity of the arch action; $V_{\rm ss}$ is the shear capacity provided by the steel shape with web concrete.

According to the simplified modified compression field theory (MCFT) (Bentz *et al*. 2006), the shear capacity of the truss action can be determined as

$$V_{\rm ct} = \beta (b - b_{\rm f}) h_0 \sqrt{f_{\rm c,outer}} \tag{2}$$

$$V_{\rm s} = \frac{A_{\rm sv} f_{\rm ys}}{s} h_0 \cot\theta \tag{3}$$

The coefficient $\beta$ in the Eq. (2) can be calculated as

$$\beta = \frac{0.4}{1 + 1500\varepsilon_{\rm x}} \times \frac{1300}{1000 + s_{\rm ze}} \tag{4}$$

where $\varepsilon_{\rm x}$ is the average longitudinal strain at the mid-depth of the cross section which can be determined by Eq. (5); $s_{\rm ze}$ is the effective crack spacing, $s_{\rm ze}$ = 300 mm.

$$\varepsilon_{\rm x} = \frac{0.5(V_{ct} + V_s)\cos\theta + \dfrac{(V_{ct} + V_s)a}{2h_0}}{2E_s A_s} \tag{5}$$

The crack angle $\theta$ can be determined by different models, but most of them are based on iteration or

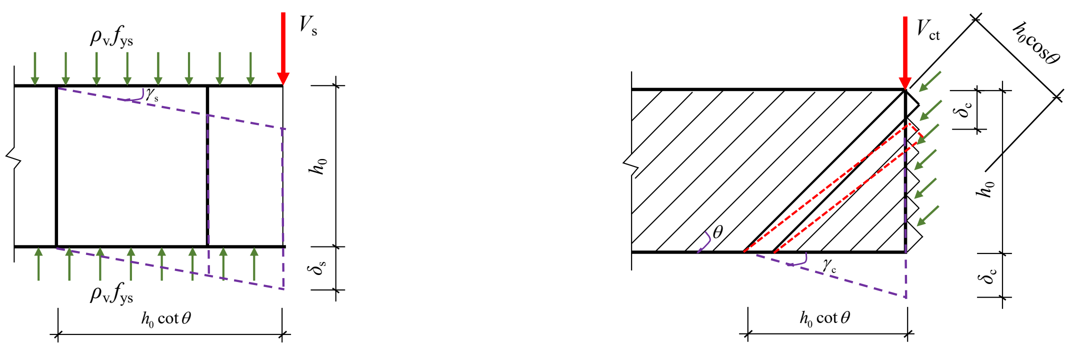


(a) Shear deformation of stirrup (b) Shear deformation of concrete

Fig. 9 Shear deformation of truss action (Pan and Li 2013) regression analysis. The formula proposed by Kim and Mander (2007), which is based on the minimum energy principle and calibrated by experimental results, is employed here, as shown in Eq. (6)

$$\theta = \tan^{-1}\left(\frac{0.6n\rho_v + 0.57\dfrac{\rho_v A_v}{\rho_s A_g}}{1+4n\rho_v}\right)^{0.25} \tag{6}$$

Therefore, the shear capacity of the truss action can be determined by solving the resulting Eqs. (2)-(6) simultaneously.

According to the Pan and Li model, the contribution of arch action to the shear capacity of the RC part can be determined by the compatibility condition as

$$\frac{V_{\mathrm{ct}}+V_{\mathrm{s}}}{K_{\mathrm{t}}} = \frac{V_{\mathrm{a}}}{K_{\mathrm{a}}} \tag{7}$$

where the $K_{\mathrm{a}}$ and $K_{\mathrm{t}}$ are the shear stiffness of the arch action and truss action, respectively.

As illustrated in Fig. 9, the shear stiffness of the truss action is

$$K_{\mathrm{t}} = \frac{V_{\mathrm{ct}}+V_{\mathrm{s}}}{(\gamma_{\mathrm{s}}+\gamma_{\mathrm{c}})} = \frac{n\rho_{\mathrm{v}}E_{\mathrm{c}}(b-b_{\mathrm{f}})h_0\cot^2\theta}{1+n\rho_{\mathrm{v}}\csc^4\theta} \tag{8}$$

Similarly, as illustrated in Fig. 10, the shear stiffness of the arch action is

$$K_{\mathrm{a}} = \frac{V_{\mathrm{a}}}{\delta_{\mathrm{a}}/a} = E_{\mathrm{c}}(b-b_{\mathrm{f}})c_{\mathrm{a}}\sin^2\alpha\cos^2\alpha \tag{9}$$

where $c_{\mathrm{a}}$ is the depth of shear compression area, namely the depth of the arch. The traditional truss-arch model defined the $c_{\mathrm{a}}$ as the half of the beam height for simplification, which does not match the experimental observation (Pan and Li 2013). This paper employed the value of $c_{\mathrm{a}}$ proposed by Choi and Park (2007) based on sectional analysis and regression analysis. The expression of $c_{\mathrm{a}}$ is as follows

$$c_a = \frac{(1-0.43\lambda)}{2(1-\frac{1}{3}\zeta)f_{\mathrm{c,outer}}}\left[\sqrt{[\varepsilon_0 E_s(\rho_s+\rho_w)]^2 + 2(1-\frac{1}{3}\zeta)f_{\mathrm{c,outer}}\varepsilon_0 E_s h_0^2(2\rho_s+\rho_w)} - \varepsilon_0 E_s h_0(\rho_s+\rho_w)\right] \geq 0 \tag{10}$$

$$\zeta = (1-0.44\lambda) \geq 0.2 \tag{11}$$

Therefore, the shear capacity of the RC part of a SRC beam is

$$V_{\mathrm{RC}} = (V_{\mathrm{ct}}+V_{\mathrm{s}}+V_{\mathrm{a}}) = (V_{\mathrm{ct}}+V_{\mathrm{s}})(1+K_{\mathrm{a}}/K_{\mathrm{t}}) \tag{12}$$

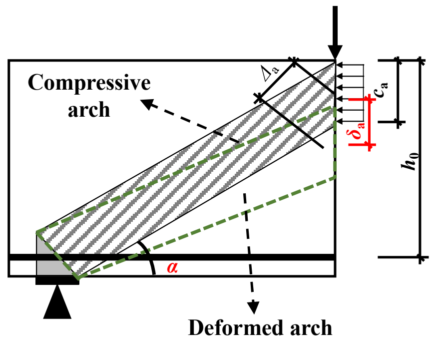


Fig. 10 Shear deformation of arch action (Pan and Li 2013)

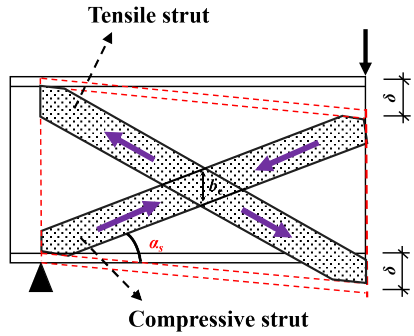


Fig. 11 Shear deformation of steel shape with web concrete

The estimated shear mechanism of the steel shape with web concrete is illustrated by Nakamura and Narita (2003) in Fig. 11. The steel web is deformed to a parallelogram and two diagonal struts are formed in the steel web, namely the tensile strut of steel and the compressive strut of concrete. The steel tensile strut and the concrete compressive strut could form an X-truss, as shown in Fig. 11. The shear capacity $V_{\mathrm{ss}}$ is the sum of the tensile strut component and the compressive strut component

$$V_{\mathrm{ss}} = f_{\mathrm{y}}b_{\mathrm{e}}t_{\mathrm{w}}\sin\alpha_{\mathrm{s}} + f_{\mathrm{c,inner}}b_{\mathrm{e}}(b_{\mathrm{f}}-t_{\mathrm{w}})\sin\alpha_{\mathrm{s}} \tag{13}$$

where $b_{\mathrm{e}}$ is the effective width of the strut. Based on the study conducted by Nakamura and Narita (2003) and the measured effective web height in the test (mean value about 35% of the web height for SC-0 to SC-4), the $b_{\mathrm{e}}$ is recommended as 2/5 of the height of the steel web in this paper because of the stronger confinement of the concrete to the steel shape in SRC beams than in PEC beams, namely $b_{\mathrm{e}} = 0.4h_{\mathrm{w}}$.

The shear stiffness of steel shape with web concrete can be expressed as

$$K_{\mathrm{s}} = K_{\mathrm{ss}} + K_{\mathrm{wc}} = G_{\mathrm{s}}A_{\mathrm{ss}} + G_{\mathrm{wc}}A_{\mathrm{wc}} \tag{14}$$

where $K_{\mathrm{s}}$ is the shear stiffness of steel shape with web concrete; $K_{\mathrm{ss}}$ and $K_{\mathrm{wc}}$ are the shear stiffness of steel web and web concrete, respectively; $G_{\mathrm{s}}$ and $G_{\mathrm{wc}}$ are the shear modulus of steel web and web concrete, respectively; $A_{\mathrm{ss}}$ and $A_{\mathrm{wc}}$ are the area of steel web and web concrete, respectively.

Table 3 Details of 75 shear-critical SRC beams

| No. | Reference | Specimen ID | $\lambda$ | $f_c$ (MPa) | | | $\rho_{ss}$ (%) | $V_e$ (kN) | $V_{c\text{-proposed}}$ (kN) | $V_{c\text{-proposed}}/V_e$ | $V_{c\text{-JGJ}}$ (kN) | $V_{c\text{-JGJ}}/V_e$ | $V_{c\text{-AISC}}$ (kN) | $V_{c\text{-AISC}}/V_e$ |
|---|---|---|---|---|---|---|---|---|---|---|---|---|---|---|
| | | | | Outer | Inner | | | | | | | | | |
| 1 | This paper | PSRC-1 | 1.0 | 36.00 | 19.44 | C | 3.46 | 2170 | 2311 | 1.07 | 1749 | 0.81 | 1321 | 0.61 |
| 2 | | PSRC-2 | 1.5 | 36.00 | 19.44 | C | 3.46 | 1600 | 1605 | 1.00 | 1321 | 0.83 | 1307 | 0.82 |
| 3 | Yang (2017) | PSRC-2-1 | 1.0 | 43.20 | 30.48 | C | 4.29 | 512 | 460 | 0.90 | 324 | 0.63 | 242 | 0.47 |
| 4 | | PSRC-2-2 | 1.5 | 43.20 | 30.48 | C | 4.29 | 375 | 318 | 0.85 | 249 | 0.67 | 239 | 0.64 |
| 5 | | PSRC-2-3 | 1.8 | 43.20 | 30.48 | C | 4.29 | 310 | 255 | 0.82 | 222 | 0.72 | 239 | 0.77 |
| 6 | | PSRC-2-4 | 1.5 | 43.20 | 17.36 | C | 4.29 | 316 | 287 | 0.91 | 235 | 0.74 | 239 | 0.76 |
| 7 | | PSRC-2-5 | 1.5 | 43.20 | 54.40 | C | 4.29 | 393 | 375 | 0.95 | 262 | 0.67 | 239 | 0.61 |
| 8 | | SRC-2-6 | 1.5 | 54.40 | 54.40 | C | 4.29 | 382 | 376 | 0.99 | 272 | 0.71 | 246 | 0.65 |
| 9 | Zheng (2011) | SRC-18 | 1.0 | 69.10 | | H | 5.61 | 475 | 453 | 0.95 | 357 | 0.75 | 287 | 0.60 |
| 10 | | SRC-19 | 1.5 | 69.10 | | H | 5.61 | 310 | 330 | 1.07 | 285 | 0.92 | 286 | 0.92 |
| 11 | | SRC-24 | 1.5 | 73.20 | | H | 5.61 | 350 | 339 | 0.97 | 292 | 0.83 | 287 | 0.82 |
| 12 | | SRC-25 | 1.5 | 82.90 | | H | 5.61 | 345 | 353 | 1.02 | 303 | 0.88 | 291 | 0.84 |
| 13 | Xue (2011) | SRRC-1 | 1.2 | 31.92 | | R | 6.03 | 318 | 352 | 1.11 | 260 | 0.82 | 238 | 0.75 |
| 14 | | SRRC-2 | 1.6 | 31.90 | | R | 6.03 | 239 | 255 | 1.07 | 209 | 0.87 | 236 | 0.99 |
| 15 | | SRRC-3 | 2.1 | 31.92 | | R | 6.03 | 184 | 184 | 1.00 | 176 | 0.95 | 235 | 1.27 |
| 16 | | SRRC-4 | 1.2 | 32.80 | | R | 6.03 | 343 | 354 | 1.03 | 261 | 0.76 | 238 | 0.69 |
| 17 | | SRRC-5 | 1.6 | 32.80 | | R | 6.03 | 245 | 257 | 1.05 | 210 | 0.86 | 236 | 0.96 |
| 18 | | SRRC-6 | 2.1 | 32.80 | | R | 6.03 | 172 | 185 | 1.08 | 177 | 1.03 | 235 | 1.37 |
| 19 | | SRRC-7 | 1.2 | 33.52 | | R | 6.03 | 324 | 356 | 1.10 | 262 | 0.81 | 239 | 0.74 |
| 20 | | SRRC-8 | 1.6 | 33.52 | | R | 6.03 | 245 | 258 | 1.05 | 211 | 0.86 | 237 | 0.97 |
| 21 | | SRRC-9 | 2.1 | 33.52 | | R | 6.03 | 178 | 186 | 1.05 | 177 | 1.00 | 235 | 1.32 |
| 22 | | SRRC-10 | 1.2 | 41.12 | | R | 6.03 | 368 | 372 | 1.01 | 273 | 0.74 | 242 | 0.66 |
| 23 | | SRRC-11 | 1.2 | 43.36 | | R | 6.03 | 368 | 377 | 1.02 | 276 | 0.75 | 243 | 0.66 |
| 24 | | SRRC-12 | 1.2 | 30.88 | | R | 6.03 | 343 | 350 | 1.02 | 258 | 0.75 | 237 | 0.69 |
| 25 | Wang (2006) | SBI-1 | 1.2 | 36.00 | | C | 7.32 | 400 | 355 | 0.89 | 282 | 0.70 | 260 | 0.65 |
| 26 | | SBI-2 | 1.8 | 36.00 | | C | 7.32 | 260 | 241 | 0.93 | 210 | 0.81 | 258 | 0.99 |
| 27 | | SBI-3 | 2.3 | 36.00 | | C | 7.32 | 240 | 171 | 0.71 | 171 | 0.71 | 257 | 1.07 |
| 28 | | SBI-4 | 2.9 | 36.00 | | C | 7.32 | 170 | 151 | 0.89 | 146 | 0.86 | 257 | 1.51 |
| 29 | | SBI-5 | 1.1 | 36.00 | | C | 6.13 | 380 | 343 | 0.90 | 293 | 0.77 | 255 | 0.67 |
| 30 | | SBI-6 | 1.8 | 36.00 | | C | 6.13 | 240 | 204 | 0.85 | 205 | 0.85 | 252 | 1.05 |
| 31 | | SBI-7 | 2.4 | 36.00 | | C | 6.13 | 200 | 141 | 0.71 | 165 | 0.82 | 251 | 1.26 |
| 32 | Shao (2007) | B1-1.0 | 0.9 | 31.50 | | L | 5.75 | 509 | 399 | 0.78 | 330 | 0.65 | 254 | 0.50 |
| 33 | | B1-1.5 | 1.4 | 31.50 | | L | 5.75 | 304 | 290 | 0.95 | 244 | 0.80 | 250 | 0.82 |
| 34 | | B1-2.0 | 1.8 | 31.50 | | L | 5.75 | 323 | 213 | 0.65 | 198 | 0.60 | 248 | 0.75 |
| 35 | | B1-2.5 | 2.3 | 31.50 | | L | 5.75 | 219 | 161 | 0.74 | 168 | 0.77 | 247 | 1.13 |
| 36 | | B1-1.5p | 1.4 | 36.72 | | L | 5.75 | 367 | 336 | 0.92 | 265 | 0.72 | 253 | 0.69 |
| 37 | | B1-2.5p | 2.3 | 36.72 | | L | 5.75 | 285 | 173 | 0.61 | 183 | 0.64 | 250 | 0.88 |
| 38 | | B2-1.0 | 0.9 | 39.80 | | L | 5.75 | 495 | 436 | 0.88 | 345 | 0.70 | 258 | 0.52 |
| 39 | | B2-1.5 | 1.4 | 39.80 | | L | 5.75 | 342 | 317 | 0.93 | 257 | 0.75 | 254 | 0.74 |
| 40 | | B2-2.0 | 1.8 | 39.80 | | L | 5.75 | 255 | 233 | 0.92 | 209 | 0.82 | 252 | 0.99 |
| 41 | | B2-2.5 | 2.3 | 39.80 | | L | 5.75 | 249 | 177 | 0.71 | 177 | 0.71 | 251 | 1.01 |
| 42 | | B3-1.0 | 0.9 | 52.30 | | L | 5.75 | 467 | 491 | 1.05 | 366 | 0.78 | 264 | 0.57 |
| 43 | | B3-1.5 | 1.4 | 52.30 | | L | 5.75 | 373 | 357 | 0.96 | 274 | 0.73 | 260 | 0.70 |
| 44 | | B3-2.0 | 1.8 | 52.30 | | L | 5.75 | 322 | 263 | 0.82 | 223 | 0.69 | 258 | 0.80 |
| 45 | | B3-2.5 | 2.3 | 52.30 | | L | 5.75 | 293 | 200 | 0.68 | 189 | 0.65 | 257 | 0.88 |

Table 3 Continued

| No. | Reference | Specimen ID | $\lambda$ | $f_c$ (MPa) Outer | Inner | | $\rho_{ss}$ (%) | $V_e$ (kN) | $V_{c\text{-proposed}}$ (kN) | $V_{c\text{-proposed}}$ $/V_e$ | $V_{c\text{-JGJ}}$ (kN) | $V_{c\text{-JGJ}}/V_e$ | $V_{c\text{-AISC}}$ (kN) | $V_{c\text{-AISC}}$ $/V_e$ |
|---|---|---|---|---|---|---|---|---|---|---|---|---|---|---|
| 46 | | B1-1a | 1.5 | 25.45 | | C | 2.70 | 356 | 298 | 0.84 | 187 | 0.53 | 173 | 0.49 |
| 47 | | B1-1b | 2.0 | 25.45 | | C | 2.70 | 349 | 183 | 0.52 | 157 | 0.45 | 170 | 0.49 |
| 48 | | B1-2a | 1.0 | 23.39 | | C | 2.70 | 368 | 464 | 1.26 | 234 | 0.64 | 178 | 0.48 |
| 49 | | B1-2b | 2.0 | 23.39 | | C | 2.70 | 147 | 132 | 1.22 | 153 | 1.04 | 168 | 1.14 |
| 50 | | B2-1a | 1.5 | 15.72 | | C | 2.70 | 248 | 285 | 1.15 | 171 | 0.69 | 172 | 0.69 |
| 51 | | B2-1b | 2.0 | 15.72 | | C | 2.70 | 203 | 179 | 0.88 | 145 | 0.71 | 168 | 0.83 |
| 52 | | B2-2a | 1.0 | 23.11 | | C | 2.70 | 376 | 473 | 1.26 | 241 | 0.64 | 186 | 0.49 |
| 53 | | B2-2b | 3.0 | 23.11 | | C | 2.70 | 168 | 133 | 0.79 | 127 | 0.75 | 172 | 1.02 |
| 54 | | B3-1a | 1.5 | 20.94 | | C | 2.70 | 318 | 318 | 1.00 | 198 | 0.62 | 190 | 0.60 |
| 55 | | B3-1b | 2.0 | 20.94 | | C | 2.70 | 249 | 206 | 0.83 | 169 | 0.68 | 186 | 0.75 |
| 56 | | B3-2a | 1.0 | 16.17 | | C | 2.70 | 318 | 469 | 1.48 | 232 | 0.73 | 192 | 0.60 |
| 57 | | B3-2b | 3.0 | 16.17 | | C | 2.70 | 137 | 142 | 1.04 | 129 | 0.94 | 178 | 1.30 |
| 58 | | B6-1a | 1.5 | 21.51 | | C | 4.91 | 426 | 330 | 0.78 | 251 | 0.59 | 282 | 0.66 |
| 59 | | B6-1b | 2.0 | 21.51 | | C | 4.91 | 331 | 215 | 0.65 | 204 | 0.62 | 279 | 0.84 |
| 60 | SCUT (1994) | B6-2a | 1.0 | 24.23 | | C | 4.91 | 501 | 519 | 1.04 | 345 | 0.69 | 292 | 0.58 |
| 61 | | B6-2b | 3.0 | 24.23 | | C | 4.91 | 211 | 152 | 0.72 | 157 | 0.74 | 278 | 1.32 |
| 62 | | B7-1a | 1.5 | 19.73 | | C | 4.91 | 418 | 336 | 0.80 | 254 | 0.61 | 288 | 0.69 |
| 63 | | B7-1b | 2.0 | 19.73 | | C | 4.91 | 321 | 222 | 0.69 | 208 | 0.65 | 285 | 0.89 |
| 64 | | B7-2a | 1.0 | 23.46 | | C | 4.91 | 518 | 527 | 1.02 | 351 | 0.68 | 299 | 0.58 |
| 65 | | B7-2b | 3.0 | 23.46 | | C | 4.91 | 206 | 162 | 0.79 | 163 | 0.79 | 285 | 1.38 |
| 66 | | B8-1a | 1.5 | 23.27 | | C | 4.91 | 442 | 368 | 0.83 | 276 | 0.62 | 305 | 0.69 |
| 67 | | B8-1b | 2.0 | 23.27 | | C | 4.91 | 334 | 249 | 0.75 | 228 | 0.68 | 301 | 0.90 |
| 68 | | B8-1a' | 1.5 | 17.31 | | C | 4.91 | 349 | 348 | 1.00 | 261 | 0.75 | 299 | 0.86 |
| 69 | | B8-1b' | 2.0 | 17.31 | | C | 4.91 | 294 | 235 | 0.80 | 216 | 0.73 | 296 | 1.01 |
| 70 | | B8-2a | 1.0 | 18.66 | | C | 4.91 | 501 | 526 | 1.05 | 349 | 0.70 | 307 | 0.61 |
| 71 | | B8-2b | 3.0 | 18.66 | | C | 4.91 | 208 | 171 | 0.82 | 169 | 0.81 | 293 | 1.41 |
| 72 | | B9-1a | 1.5 | 17.02 | | C | 4.91 | 430 | 338 | 0.79 | 237 | 0.55 | 263 | 0.61 |
| 73 | | B9-1b | 2.0 | 17.02 | | C | 4.91 | 339 | 227 | 0.67 | 198 | 0.58 | 259 | 0.76 |
| 74 | | B9-2a | 1.0 | 19.09 | | C | 7.50 | 535 | 587 | 1.10 | 451 | 0.84 | 412 | 0.77 |
| 75 | | B9-2b | 3.0 | 19.09 | | C | 7.50 | 243 | 204 | 0.84 | 203 | 0.84 | 398 | 1.64 |
| Average ratio of measured to calculated value | | | | | | | | | | 0.92 | | 0.74 | | 0.84 |
| Coefficient of variation | | | | | | | | | | 0.18 | | 0.15 | | 0.32 |

*The label "C" means conventional concrete; the label "H" means high-strength concrete; the label "R" means recycled aggregate concrete; the label "L" means lightweight aggregate concrete

As well known, brittle failure would occur in reinforced concrete beams, indicating that a sharp decrease could be observed in load-displacement curves after the peak load reached. Nevertheless, PEC members can exhibit great toughness during the post-peak period, indicating that the peak load of PEC members can be hold nearly without descending (He *et al*. 2012). Therefore, if the $(V_{ss}/K_s) < [V_{RC}/(K_a+K_t)]$, the steel shape with web concrete can reach the corresponding peak load first and then hold the peak load for a long time, indicating that the shear capacity of a SRC beam can be regarded as the sum of the shear capacity of RC part and that of steel shape with web concrete part. If $(V_{ss}/K_s) > [V_{RC}/(K_a+K_t)]$, the RC part can reach the corresponding peak load first and then suffer a sharp decrease in load-bearing capacity, indicating that the sum of the shear capacity of RC part and that of steel shape with web concrete part will overestimate the shear capacity of the entire SRC beam. In this case, a reduction coefficient should be employed for safety.

Therefore, the shear capacity of a SRC beam can be determined by solving Eqs. (1), (12), (13) simultaneously, and a reduction coefficient should be employed if $(V_{ss}/K_s) > [V_{RC}/(K_a+K_t)]$. Because the $f_{c,outer}$ in Eq. (2) and Eq. (10) is the compressive strength of concrete in the precast outer-part, and $f_{c,inner}$ in Eq. (13) is the compressive strength of concrete in the cast-in-place inner-part, the proposed model can effectively consider the different concrete strengths of the precast outer-part and cast-in-place inner-part and is

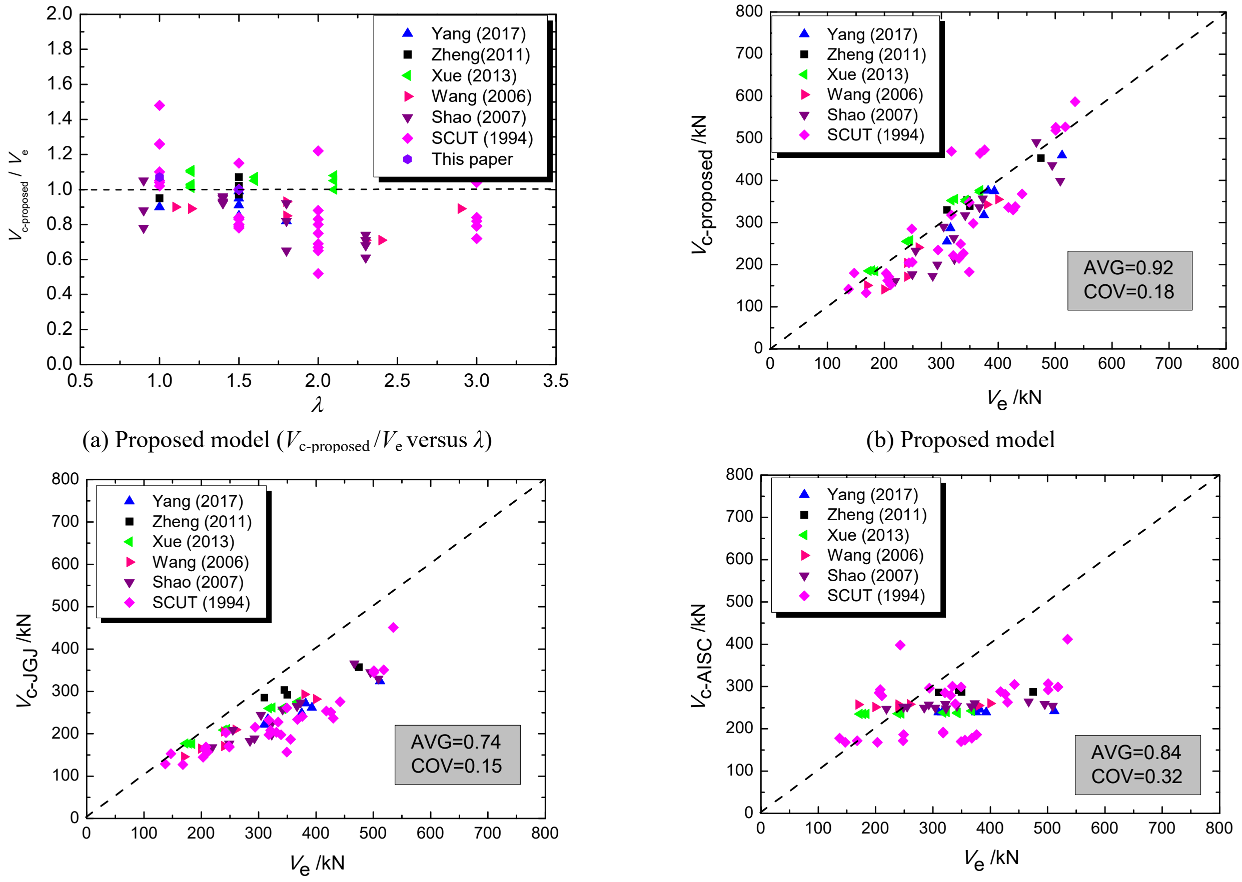


(a) Proposed model ($V_{\text{c-proposed}}/V_{\text{e}}$ versus $\lambda$) (b) Proposed model

(c) JGJ 138 model (d) AISC 360 model

Fig. 12 Comparison of calculated and experimental shear capacity

also suitable for predicting the shear capacity of conventional cast-in-place SRC beams ($f_{c,\text{outer}} = f_{c,\text{inner}}$).

## 5. Validation

A compiled experimental database of 75 shear-critical PSRC and SRC beams was used to evaluate the proposed model and the models from AISC 360 and JGJ 138. In the database, the concrete contains conventional concrete, recycled aggregate concrete, lightweight aggregate concrete and high-strength concrete. The compressive strength of concrete varies from 15.7 MPa to 82.9 MPa. The height of beam varies from 240 mm to 650 mm. The steel shape ratio varies from 2.70% to 7.50%. Table 3 tabulates the ratio of calculated to measured shear capacity of these models, and the mean ratio of calculated to measured shear capacity and its coefficient of variation are 0.92 and 0.18, 0.84 and 0.32, 0.74 and 0.15 for the proposed model, AISC 360 model and JGJ 138 model, respectively. As can be seen from Table 3 and Fig. 12, the proposed model can represent the shear capacity reasonably, although it slightly underestimates the shear capacity, and the predicted shear capacities by the AISC 360 model and JGJ 138 model are relatively conservative.

The concrete type played an important role in predicting the shear capacity of SRC beams. The mean ratio of calculated to measured shear capacity and its coefficient of variation are 0.91 and 0.20, 1.00 and 0.05, 1.04 and 0.03, 0.82 and 0.13 for the conventional concrete, high-strength concrete, recycled aggregate concrete and lightweight aggregate concrete, indicating that the best prediction occurred in the specimens with high-strength concrete and the worst prediction occurred in the specimens with lightweight aggregate concrete. Because the number of specimens with high-strength was limited, further work should be conducted to search more available data of SRC beams with high-strength concrete. Additionally, the shear capacity of specimens with lightweight aggregate concrete was generally underestimated, therefore, further work should be conducted to put forward a modified model which can take the concrete types into account.

As shown in Fig. 13, the first case mentioned in the previous section, namely ($V_{ss}/K_s$) < [$V_{RC}/(K_a+K_t)$], can be found in all the specimens of the database. The reason is that the steel shape with wide-width flange or medium-width flange is widely applied in SRC members for higher capacity and greater rigidity, the shear stiffness and capacity of steel shape with web concrete are usually larger than that of RC part. In the future, more test data of the specimens with low steel ratios should be collected to verify the second case mentioned before.

Fig. 14 shows the relationship between the height of shear compression area, which can be calculated by Eq.

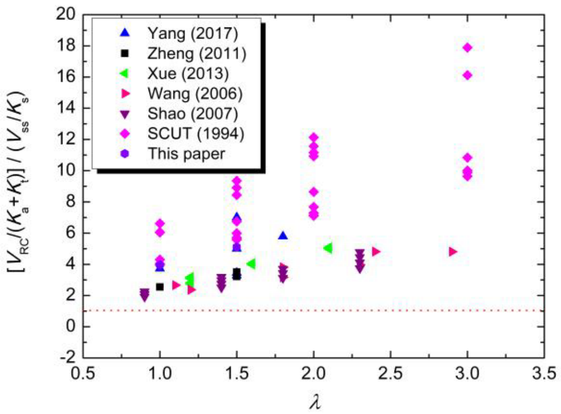


Fig. 13 Comparison of calculated shear capacity of each part

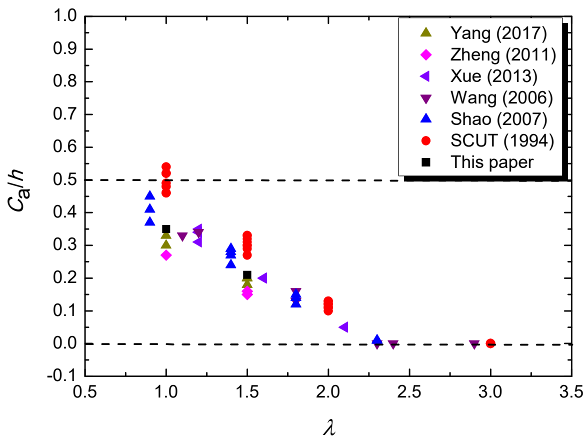


Fig. 14 Height of shear compression area versus aspect ratio

(10), and the aspect ratio. The data trend suggests that height of shear compression area decreases with the increasing of the aspect ratio, indicating that the arch action may be weakened by the decreasing height of the arch and the decreasing angle between the arch and longitudinal axis. It also indicates that the traditional truss-arch model proposed by Ichinose (1992) may overestimate that contribution provided by the arch action.

## 6. Conclusions

This study presented the results of a static test on two full-scale precast steel reinforced concrete (PSRC) beams. The main parameter examined in this study was the shear span aspect ratio. Based on the test results, an analytical model was proposed to calculate the shear capacity of PSRC and SRC beams. The following conclusions can be drawn:

- The shear span aspect ratio directly affects the failure modes and shear capacities of the PSRC beams. Both the two specimens failed in anticipated shear failure, in which the specimen PSRC-1 with lower aspect ratio failed in diagonal compression failure with lower ductility ratio and the specimen PSRC-2 with higher aspect ratio failed in shear compression failure with excellent deformability. No obvious longitudinal cracks which indicated slippage occurred were observed during the final loading stages, indicating that the precast concrete and cast-in-place concrete were well composite in these specimens.
- Based on the test results, an analytical model was proposed to analyze the shear mechanisms of PSRC and SRC beams. In the proposed model, the overall shear capacity of the specimens can be determined by combining the shear capacity of steel shape with web concrete determined by modified Nakamura and Narita model and the shear capacity of reinforced concrete part determined by compatible truss-arch model which can consider both the contributions of concrete and stirrups to shear capacity in the truss action as well as the contribution of arch action through compatibility of deformation.
- In the proposed model, the shear capacity of SRC beams can be determined though the comparison of the peak shear deformation of reinforced concrete part, $[V_{RC}/(K_a+K_t)]$, and that of steel shape with web concrete part, $(V_{ss}/K_s)$. If $(V_{ss}/K_s) < [V_{RC}/(K_a+K_t)]$, the overall shear capacity of a SRC beam can be regarded as the sum of the shear capacity of reinforced concrete part and that of steel shape with web concrete part. If not, a reduction coefficient should be employed for safety.
- From the comparison of measured and predicted shear capacities of 75 shear-critical PSRC and SRC beams, the shear capacity predicted by the proposed model is found to agree well with experimental results, and the mean ratio of calculated to measured shear capacity and its coefficient of variation are 0.92 and 0.18, respectively. Both the AISC 360 model and JGJ 138 model relatively underestimate the shear capacity of PSRC and SRC beams. The concrete type played an important role in predicting the shear capacity of SRC beams, and the best prediction occurred in the specimens with high-strength concrete and the worst prediction occurred in the specimens with lightweight aggregate concrete using the proposed model. Therefore, further work should be conducted to put forward a modified model which can take the concrete types into account.

## Acknowledgments

The experiments are sponsored by the National Key Research and Development Program of China (Grant No. 2017YFC0703404), the National Natural Science Foundation of China (Grant No. 51478287 and No. 51578443), Potential Excellent PhD Dissertation Foundation of Xi'an University of Architecture and Technology (Grant No. 1601110035). The supports are greatly appreciated. Additionally, financial support from the

China Scholarship Council (CSC) for Yicong Xue's research at QUB, as a visiting researcher, is highly appreciated.

## References

AISC 360-10 (2010), Specification for structural steel buildings, American Institute of Steel Construction; Chicago, IL, USA.

Bentz, E.C., Vecchio, F.J. and Collins, M.P. (2006), "Simplified modified compression field theory for calculating shear strength of reinforced concrete elements", *ACI Struct. J.*, **103**(4), 614-624.

Chen, Z. and Liu, X. (2018), "Seismic behavior of steel reinforced concrete cross-shaped column under combined torsion", *Steel Compos. Struct., Int. J.*, **26**(4), 407-420. http://dx.doi.org/10.12989/scs.2018.26.4.407

Choi, K.K. and Park, H.G. (2007), "Unified shear strength model for reinforced concrete beams - part ii: verification and simplified method", *ACI Struct. J.*, **104**(2), 153-161.

Chu, L., Li, D., Ma, X. and Zhao, J. (2018), "Cyclic behaviour of concrete encased steel (CES) column-steel beam joints with concrete slabs", *Steel Compos. Struct., Int. J.*, **29**(6), 735-748. http://dx.doi.org/10.12989/scs.2018.29.6.735

Deng, M., Ma, F., Ye, W. and Liang, X. (2018), "Investigation of the shear strength of HDC deep beams based on a modified direct strut-and-tie model", *Constr. Build. Mater.*, **172**, 340-348. https://doi.org/10.1016/j.conbuildmat.2018.03.274

Elmy, M.H. and Nakamura, S. (2017), "Static and seismic behaviours of innovative hybrid steel reinforced concrete bridge", *J. Constr. Steel Res.*, **138**, 701-713. https://doi.org/10.1016/j.jcsr.2017.08.025

GB 50010-2010 (2010), Code for Design of Concrete Structures, MoHURD; Beijing, China. [In Chinese]

He, J., Liu, Y., Chen, A. and Yoda, T. (2012), "Shear behavior of partially encased composite i-girder with corrugated steel web: experimental study", *J. Constr. Steel Res.*, **77**, 193-209. https://doi.org/10.1016/j.jcsr.2012.05.005

Huang, Z., Huang, X., Li, W., Mei, L. and Liew, J.Y. (2019), "Experimental behavior of VHSC encased composite stub column under compression and end moment", *Steel Compos. Struct., Int. J.*, **31**(1), 69-83. http://dx.doi.org/10.12989/scs.2019.31.1.069

Ichinose, T. (1992), "A shear design equation for ductile RC members", *Earthq. Eng. Struct. Dyn.*, **21**(3), 197-214. https://doi.org/10.1002/eqe.4290210302

JGJ 138-2016 (2016), Code for design of composite structures, MoHURD; Beijing, China. [In Chinese]

Kim, J.H. and Mander, J.B. (2007), "Influence of transverse reinforcment on elastic shear stiffness of cracked concrete elements", *Eng. Struct.*, **29**(8), 1798-1807. https://doi.org/10.1016/j.engstruct.2006.10.001

Kim, S., Hong, W.K., Kim, J.H. and Kim, J.T. (2013), "The development of modularized construction of enhanced precast composite structural systems (smart green frame) and its embedded energy efficiency", *Energy Build.*, **66**(5), 16-21. https://doi.org/10.1016/j.enbuild.2013.07.023

Liang, J., Zhang, G., Wang, J. and Hu, M. (2019), "Mechanical behaviour of partially encased composite columns confined by CFRP under axial compression", *Steel Compos. Struct., Int. J.*, **31**(2), 125-131. http://dx.doi.org/10.12989/scs.2019.31.2.125

Ma, H., Xue, J., Liu, Y. and Dong, J. (2016), "Numerical analysis and horizontal bearing capacity of steel reinforced recycled concrete columns", *Steel Compos. Struct., Int. J.*, **22**(4), 797-820. http://dx.doi.org/10.12989/scs.2016.22.4.797

Massone, L.M., Sayre, B.L. and Wallace, J.W. (2017), "Load-deformation responses of slender structural steel reinforced concrete walls", *Eng. Struct.*, **140**, 77-88. https://doi.org/10.1016/j.engstruct.2017.02.050

Nakamura, S.I. and Narita, N. (2003), "Bending and shear strengths of partially encased composite I-girders", *J. Constr. Steel Res.*, **59**(12), 1435-1453. https://doi.org/10.1016/S0143-974X(03)00104-4

Nzabonimpa, J.D., Hong, W.K. and Kim, J. (2017), "Nonlinear finite element model for the novel mechanical beam-column joints of precast concrete-based frames", *Comput. Struct.*, **189**, 31-48. https://doi.org/10.1016/j.compstruc.2017.04.016

Nzabonimpa, J.D., Hong, W.K. and Kim, J. (2018), "Strength and post-yield behavior of T-section steel encased by structural concrete", *Struct. Des. Tall Special Build.*, **27**(5), 1-25. https://doi.org/10.1002/tal.1447

Pan, Z. and Li, B. (2013), "Truss-arch model for shear strength of shear-critical reinforced concrete columns", *J. Struct. Eng.*, **139**(4), 548-560. https://doi.org/10.1061/(ASCE)ST.1943-541X.0000677

Park, R. (1988), "State of the art report ductility evaluation from laboratory and analytical testing", *Proceedings of 9th World Conference on Earthquake Engineering*, Tokyo, Japan, August.

Rana, M.M., Lee, C.K., Al-Deen, S. and Zhang, Y.X. (2018), "Flexural behaviour of steel composite beams encased by engineered cementitious composites", *J. Constr. Steel Res.*, **143**, 279-290. https://doi.org/10.1016/j.jcsr.2018.01.004

Xiao, C., Deng, F., Chen, T. and Zhao, Z. (2017), "Experimental study on concrete-encased composite columns with separate steel sections", *Steel Compos. Struct., Int. J.*, **23**(4), 483-491. http://dx.doi.org/10.12989/scs.2017.23.4.483

Yan, B., Liu, J. and Zhou, X. (2017), "Axial load behavior and stability strength of circular tubed steel reinforced concrete (SRC) columns", *Steel Compos. Struct., Int. J.*, **25**(5), 545-556. http://dx.doi.org/10.12989/scs.2017.25.5.545

Yang, Y., Yu, Y., Guo, Y., Roeder, C.W., Xue, Y. and Shao, Y. (2016), "Experimental study on shear performance of partially precast castellated steel reinforced concrete (CPSRC) beams", *Steel Compos. Struct., Int. J.*, **21**(2), 289-302. http://dx.doi.org/10.12989/scs.2016.21.2.289

Yang, Y., Xue, Y., Yu, Y., Ma, N. and Shao, Y. (2017), "Experimental study on flexural performance of partially precast steel reinforced concrete beams", *J. Constr. Steel Res.*, **133**, 192-201. https://doi.org/10.1016/j.jcsr.2017.02.019

Yang, Y., Xue, Y., Yu, Y. and Gao, F. (2018), "Experimental study on seismic performance of partially precast steel reinforced concrete columns", *Eng. Struct.*, **175**, 63-75. https://doi.org/10.1016/j.engstruct.2018.08.027

Zhu, W., Jia, J. and Zhang, J. (2017), "Experimental research on seismic behavior of steel reinforced high-strength concrete short columns", *Steel Compos. Struct., Int. J.*, **25**(5), 603-615. http://dx.doi.org/10.12989/scs.2017.25.5.603

*CC*

## Notations

| | |
|---|---|
| $A_g$ | gross area of cross-section of RC part; |
| $A_s$ | cross-sectional area of tensile longitudinal rebar; |
| $A_{sv}$ | cross-sectional area of stirrup at spacing $s$; |
| $A_{ss}$ | area of steel web; |
| $A_v$ | area enclosed by stirrup; |
| $A_{wc}$ | area of web concrete; |
| $a$ | length of shear span; |
| $b$ | width of beam; |
| $b_e$ | effective width of strut in steel shape, $b_e$=0.4$h_w$; |
| $b_f$ | width of steel flange; |
| $c_a$ | depth of shear compression area; |
| $E_c$ | modulus of elasticity of concrete; |
| $E_s$ | modulus of elasticity of steel; |
| $f_{c,inner}$ | prism compressive strength of concrete in inner-part; |
| $f_{c,outer}$ | prism compressive strength of concrete in outer-part; |
| $f_y$ | yield stress of steel shape; |
| $f_{ys}$ | yield stress of stirrup; |
| $G_s$ | shear modulus of steel web; |
| $G_{wc}$ | shear modulus of web concrete; |
| $h_0$ | distance from beam top to center of tensile longitudinal rebar; |
| $h_w$ | height of steel web; |
| $K_a$ | shear stiffness of arch action; |
| $K_t$ | shear stiffness of truss action; |
| $K_s$ | shear stiffness of steel shape with web concrete; |
| $K_{ss}$ | shear stiffness of steel web; |
| $K_{wc}$ | shear stiffness of web concrete; |
| $n$ | $E_s$ /$E_c$; |
| $s$ | spacing of stirrup; |
| $s_{ze}$ | effective crack spacing; |
| $t_w$ | thickness of steel web; |
| $\alpha$ | inclination of arch in RC part; |
| $\alpha_s$ | inclination of strut in steel shape; |
| $\theta$ | angle of inclined strut in cracked concrete with respect to longitudinal axis of beam in truss action; |
| $\rho_s$ | ratio of tensile longitudinal rebar; |
| $\rho_{ss}$ | ratio of steel shape; |
| $\rho_w$ | ratio of steel web; |
| $\rho_v$ | ratio of stirrup; |
| $\lambda$ | shear span aspect ratio; |
| $\varepsilon_0$ | peak compressive strain of concrete. |